Molecular Diversity
https://doi.org/10.1007/s11030-023-10796-3

ORIGINAL ARTICLE

The identification of c-Abl inhibitors as potential agents for Parkinson's disease: a preliminary in silico approach

Emdormi Rymbai[1] · Dhritiman Roy[2] · Srikanth Jupudi[3] · Venkatesan Srinivasadesikan[4]

Received: 15 August 2023 / Accepted: 18 December 2023

Abstract

Parkinson's disease (PD) is the most common movement disorder worldwide. PD is primarily associated with the mutation, overexpression, and phosphorylation of α-synuclein. At the molecular level, the upstream protein c-Abl, a tyrosine kinase, has been shown to regulate α-synuclein activation and expression patterns. This study aimed to identify potential c-Abl inhibitors through in silico approaches. Molecular docking was performed using PyRx software, followed by Prime MM-GBSA studies. BBB permeability and toxicity were predicted using CBligand and ProTox-II, respectively. ADME was assessed using QikProp. Molecular dynamics were carried out using Desmond (Academic version). DFT calculations were performed using the Gaussian 16 suite program. The binding scores of the top hits, norimatinib, DB07326, and entinostat were − 11.8 kcal/mol, − 11.8 kcal/mol, and − 10.8 kcal/mol, respectively. These hits displayed drug-likeness with acceptable ADME properties, except for the standard, nilotinib, which violated Lipinski's rule of five. Similarly, the molecular dynamics showed that the top hits remained stable during the 100 ns simulation. DFT results indicate DB04739 as a potent reactive hit. While based on toxicity prediction, entinostat may be a potential candidate for preclinical and clinical testing in PD. Further studies are warranted to confirm the activity and efficacy of these ligands for PD.

Keywords Parkinson's disease · c-Abl · c-Abl inhibitors · Molecular docking · Molecular dynamics

Introduction

Parkinson's disease (PD) is the second most common neurodegenerative disease after Alzheimer's disease (AD). PD is the most common movement disorder and was first described by James Parkinson in his essay "The shaking palsy" [1, 2]. PD is mainly affecting the older population (2–3%) that is ≥ 65 years of age [1]. However, PD is also affecting the young population that is < 40 years of age [1]. Among the older populations, men are majorly affected when compared to women [3]. In contrast, few studies have shown that women are at a higher risk of developing PD when compared to men. These studies have shown that estrogen deficiency declines with age in women and predisposes women to PD development [3–5]. In line with these findings, recent clinical study points to the beneficial effects of estrogen in postmenopausal women [6]. People suffering from PD are associated with primary symptoms such as bradykinesia, hypokinesia, rigidity, and tremor. These symptoms appear after dopaminergic neuron loss of more than 80% [7, 8]. Secondary symptoms include defective posture (shuffling) and gait, mask-like face, and sialorrhoea, often with

Emdormi Rymbai and Dhritiman Roy have contributed equally to this work.

✉ Emdormi Rymbai
edrphd@jssuni.edu.in

Dhritiman Roy
rs_dhritimanroy@dibru.ac.in

Srikanth Jupudi
sjphd@jssuni.edu.in

Venkatesan Srinivasadesikan
vsdgun@gmail.com

[1] Department of Pharmacology, JSS College of Pharmacy, JSS Academy of Higher Education & Research, Ooty, Nilgiris, Tamil Nadu, India

[2] Department of Pharmaceutical Sciences, Faculty of Science and Engineering, Dibrugarh University, Dibrugarh, Assam, India

[3] Department of Pharmaceutical Chemistry, JSS College of Pharmacy, JSS Academy of Higher Education & Research, Ooty, Nilgiris, Tamil Nadu, India

[4] Department of Sciences and Humanities, Vignan's Foundation for Science, Technology and Research (Deemed to be University), Vadlamudi, Guntur, Andhra Pradesh, India

Published online: 25 January 2024

dementia and autonomic impairment [9]. Although several risk factors and hypotheses have been proposed to be associated with the development of PD, the etiology of PD remains largely unknown [10]. Importantly, neuro-histopathological examination has shown the selective degeneration of mesencephalic dopaminergic neurons in the substantia nigra pars compacta (SNPC) and nigrostriatal tract (striatum) [7]. This includes widespread intracellular accumulation of α-synuclein [1, 11]. In addition, excitotoxicity, mitochondrial dysfunction, oxidative stress, inflammation, and apoptosis were also reported in PD [9]. Excitotoxicity is a concept of neuronal cell death that results from the toxic actions of excitatory amino acids such as glutamate and aspartate [12, 13].

The accumulation of α-synuclein in PD is often consider central to the pathophysiology of PD [1, 11]. α-synuclein was first identified as the major contributor of PD in 1997 [10]. The loss of dopamine (DA) in PD is correlated to the loss in the normal function of α-synuclein and the mutation of several other genes such as leucine rich repeat kinase 2 (LRRK2), PTEN-Induced Kinase 1 (PINK1), Parkinson's at-risk Kinase (PARK), etc. [1, 7]. α-synuclein contribute to PD development, in part, by interfering with various process involves in dopamine signaling. α-synuclein inhibits tyrosine hydroxylase and L-aromatic amino acid decarboxylase, the key enzymes that are crucial for dopamine synthesis [14]. α-synuclein mediates the trafficking of dopamine transporter to the pre-synaptic membrane causing rapid uptake of dopamine from the synapse [14, 15]. α-synuclein also increases the dopamine oxidation by inhibiting the sequestration of dopamine inside the vesicle monoamine transporter 2 (VMAT2). α-synuclein dose this either by regulating the expression of VMAT2 or physical interaction with VMAT2 [14, 15]. α-synuclein mediates these mechanisms due to the loss of function, mutations, multiplications, and phosphorylation [7, 16, 17]. Mutations that have been so far reported to occurred in α-synuclein gene, *SNCA* are A18T, A29S, A30P, E46K, H50Q, G51D, A53T, A53E, and A53V [10, 17–19]. The mutations and multiplications (abnormal expression of α-synuclein) of *SNCA* contributes to rare forms of familial PD [20], whereas post-translational modifications such as nitrosylation, oxidation, and phosphorylation contribute to sporadic and familial forms of PD [21, 22]. Among the various post-translational modification events, phosphorylation of α-synuclein is the major contributor of PD [21, 22]. Specific mutations in other genes, for example, PARK2 (K211N, R275W, G430W, C431S) contribute to α-synuclein aggregation and mitochondrial dysfunction leading to dopaminergic degeneration [23–25].

Cellular Abelson murine leukemia viral oncogene homolog 1 (c-Abl) belongs to a family of non-receptor protein tyrosine kinases. c-Abl is localized at different subcellular sites, including the nucleus, cytoplasm, mitochondria, the endoplasmic reticulum, and the cell cortex. In these cellular compartments, c-Abl interacts with a large variety of cellular proteins. These includes signaling adaptors, kinases, phosphatases, cell-cycle regulators, transcription factors, and cytoskeletal proteins. c-Abl plays an essential role in cellular processes such as regulation of cell growth and survival, oxidative stress, DNA-damage responses, actin dynamics, and cell migration [26]. Furthermore, c-Abl is implicated in a number of human diseases such as leukemia [26], PD [27–29], and Alzheimer's disease (AD) [30]. In these diseases, c-Abl is correlated to its aberrant activation and abnormal expression. In PD, c-Abl is activated by stressors, toxins, including misfolded α-synuclein [20, 22, 31, 32]. In PD patients and animal models, c-Abl seems to interfere with the normal functioning of α-synuclein, parkin, mitogen-activated protein kinase (p38α), NACHT, LRR, and PYD domains-containing protein [nucleotide-binding domain, leucine-rich-containing family, pyrin domain-containing-3 (NLRP3)]. Mechanistically, c-Abl induces neuronal death through the activation of α-synuclein, mitogen-activated protein kinase (p38α), and NLRP3, and inhibition of parkin [27, 32, 33]. c-Abl-induced α-synuclein activation (phosphorylation) interferes with dopamine signaling [14, 27, 32, 33]. c-Abl-induced mitogen-activated protein kinase (p38α) and NLRP3 activation overwhelmed the inflammatory signaling leading to neuronal death [27, 32, 33]. Lastly, c-Abl-induced parkin inhibition aggrevate the generation of reactive oxygen species that interfere with the plasma membrane integrity [27, 32, 33]. In line with these observations, the inhibition of c-Abl in animal models and PD patients have shown promising results [27, 34–36].

Despite the above observations, some studies are have shown that c-Abl inhibitor, Nilotinib is not adequate to ameliorate the neuronal loss [37] which could be related to its inadequate CNS permeability [27]. On the other hand, Vodobatinib, a c-Abl inhibitor having better CNS penetrant, is current under phase 2 assessment (NCT03655236) for PD [27]. In light of the above observations, the aim of this study is to identify a potential c-Abl inhibitors with a potent CNS permeability by in silico techniques. The in silico techniques offer a cost-effective, rapid, and low risk in the process of drug discovery and development. Over the years, several studies have identified potent kinase inhibitors for neurodegenerative diseases using computational tools [38–40]. The objective of this study includes (i) the collection of a set of compounds that includes US-FDA approved, investigational, and experimental drugs; (ii) molecular docking studies and free energy calculation; (iii) absorption, distribution, metabolism, excretion, toxicity (ADMET), and CNS permeability prediction; (iv) molecular dynamics; and (v) density functional theory (DFT).

Materials and methods

Ligand collection and preparation

Ligands were collected from DrugBank database (https://go.drugbank.com/). Ligands were further divided into batches for high throughput virtual screening.

Protein preparation

The protein–protein data bank (PDB) (PDB ID: 3CS9) was downloaded from research collaboratory for structural bioinformatics (https://www.rcsb.org/). The protein was prepared using discovery studio visualizer (v16.1.0.15350) where unwanted chains, co-crystals, and water molecules were removed.

Ligand–receptor docking

Molecular docking for the binding affinity and ligand–protein interactions were carried out using PyRx (Ver.0.9.0). The PyRx is a tool that provides the graphic user interface for other molecular docking tools including Autodock vina. AutoDock Vina is a standalone software that requires command line for carrying molecular docking. The use of PyRx increases the usability and accessibility of Autodock Vina to a wider range of researchers (not accustomed to command line) working in the fields of molecular biology and drug development. Autodock vina is an advancement to Autodock 4.2 in terms of speed and ligand pose prediction [41]. In addition to providing thorough details regarding the binding poses of ligands at the protein's binding site, Autodock Vina uses a scoring algorithm to determine the binding energy. The prepared protein was loaded into PyRx and then converted into PDBQT. Similarly, the prepared ligands were energy minimized using open babel and converted into PDBQT file. A PDBQT file, also known as a Protein Data Bank, in Quartenary Format is an extension of PDB format which is employed to represent the three-dimensional structures of proteins and ligands. The PDBQT format provides additional information that is essential for conducting docking and virtual screening studies. The additional information provided by PDBQT includes polar hydrogen atoms, atom types, partial charges, and the flexible portions of ligand and protein [42]. Ligand–receptor docking studies were carried out against c-Abl-bound nilotinib as inhibitor. Nilotinib forms hydrogen bonds (H-bonds) with Glutamic Acid 286 (GLU286), Threonine 315 (Thr315), Methionine 318 (Met318), and Aspartic Acid 381 (Asp381). Overall, the amino acids around nilotinib including the non-H-bond were used to generate a grid box for the ligand–receptor docking. This was achieved by visualizing the 2D ligand–receptor interaction using discovery studio visualizer (v16.1.0.15350). By selecting the surrounding amino acids, a 3D grid was generated with center $x = 28.497$, $y = 3.015$, $z = 52.220$ and dimensions $x = 25.824$, $y = 22.457$, $z = 22.583$.

BBB prediction

The blood–brain barrier (BBB) prediction was carried out using CBligand (https://www.cbligand.org/CCGS/) database. CBligand is a free online database that is commonly used to predict the BBB permeability of small molecules. The database uses various computational algorithms such as TargetHunter, HTDocking, and BBB predictor for target identification and polypharmacology analysis. The database was constructed using various AD chemo-genomics data records. This includes AD-related genes (928), proteins (320), 194 US-FDA approved or under clinical trial drugs. Additionally, a total of 405,188 chemicals which were retrieved from 1,023,137 records having reported for bioactivities were included [43].

MM-GBSA

Molecular mechanics-generalized born-surface area MM-GBSA was carried out using the prime feature in Schrodinger 2021-3. MM-GBSA is a method used to calculate the contributions of enthalpy and entropy-related components toward the binding of the ligand–protein complex. The docked poses were minimized using the local optimization feature in Prime. Prime MM-GBSA was used to calculate the ligand–receptor complexes with all receptor residues being held frozen [44, 45].

The binding free energy ΔG bind is estimated as: $\Delta G\text{bind} = \Delta E_{MM} + \Delta G_{solv} + \Delta G_{SA.}$

ΔE_{MM} = difference in energy between the complex structure and the sum of the energies of the ligand and unliganded protein using the OPLS4 force field.

ΔG_{solv} = difference in the GBSA solvation energy of the complex and the sum of the solvation energies for the ligand and unliganded protein.

ΔG_{SA} = difference in the surface area energy for the complex and the sum of the surface area energies for the ligand and unliganded protein.

ADME and toxicity prediction

The physically and pharmacokinetically significant descriptors, absorption, distribution, metabolism, and excretion (ADME) for the top hits were predicted by QikProp module of Schrodinger suite. The toxicity of the drug molecules—DB04868, DB04739, DB11841, and DB07326 were

predicted by using the ProTox-II webtool (https://tox-new.charite.de/protox_II/). PROTOX-II is a web server tool that employs a curated dataset, calculating descriptors and identifying alerts for precise toxicity prediction. Additionally, ProTox-II tool that specifically determines the type of toxicities. The toxicities defined by proTox-II are divided into acute toxicity, organ toxicity, toxicological endpoints, toxicological pathways, and toxicity targets. ProTox-II utilizes different algorithms such as random forest, support vector machine, and Bernoulli–Naive Bayes algorithm to predict these toxicities [46].

Molecular dynamics

The molecular dynamics (MD) simulation for the docked protein–ligand complex was carried out using Desmond (Academic version). Briefly, the protein–ligand system was solvated in a water model (TIP4P) inside an orthorhombic water box of 10 Å. The system was neutralized by adding 0.15 M of sodium chloride to mimic the physiological condition. The system is minimized by applying optimized potentials for liquid simulations 4 (OPLS4) force field. The system is relaxed before running the simulation by a six-step protocol that is built in with the Desmond module. The system was run in a constant temperature and pressure environment (NPT). The default temperature (300 K) and 1.01325 Pa (atmospheric pressure) were also applied for the simulation. The simulation was carried out for 100 ns for each of the system. The period of simulation was decided based on the convergence of the system in the simulated environment [42, 47, 48].

Density functional theory (DFT) studies

The 3D electronic states of molecules and atoms in the context of frontier molecular orbitals density fields [highest occupied molecular orbital (E_{HOMO}) and lowest unoccupied molecular orbital (E_{LUMO})] were determined using Gaussian 16 suite program [49]. E_{HOMO} and E_{LUMO} help explain the molecular properties and biological activity of the molecules [50]. E_{HOMO} and E_{LUMO} are the main orbitals that take part in chemical stability and also details about the donor–acceptor interactions. The electron donation capability was represented by E_{HOMO} while the E_{LUMO} represents the ability to accept electron. The Eigen values of E_{HOMO} and E_{LUMO}, and their energy gap reflect the chemical reactivity, level of conductivity, and kinetic stability of the molecule. Smaller energy gap ($\Delta E_{HOMO-LUMO}$) value indicates that easier electron transfer occurs from E_{HOMO} to E_{LUMO} with a high chemical reactivity and low kinetic stability. The higher relative energy gaps indicate kinetically unstable nature of the molecule [49, 51].

Result

Molecular docking

The amino acids of c-Abl around nilotinib are used to generate a grid for molecular docking, Fig. 1. From molecular docking studies, the binding affinity (Kcal/mol) of the ligands toward the receptor is tabulated in Table 1. The top 21 ligands were chosen based on the binding affinity (Kcal/mol) and BBB permeability prediction as predicted by PyRx and CBligand server, respectively. The top ligand, DB04868, represents the co-crystal ligand, nilotinib with the binding affinity of 14.2 kcal/mol.

Further, to narrow down the best hits for MD simulation, we set three criteria. First criteria, the ligand should form the same hydrogen bonding to c-Abl when compared to nilotinib. Second criteria, the ligand should have BBB permeability as determined by Cbligand. Third criteria, the ligand should have a better or comparable binding affinity to c-Abl when compared to nilotinib. The ligand–receptor 2D interactions are mentioned in Table 1. This was done to analyzed the binding of ligands with critical amino acids of c-Abl. Insight visualization into the ligand–receptor 2D interactions shows that three ligands bearing DrudBank ID DB04739, DB07326, and DB11841 form identical H-bond with key amino acids that interact with co-crystal ligand, nilotinib (Fig. 2). The 3D interactions have been given in the supplementary (Fig. S1). Interestingly, DB17141 (Vodobatinib), a potent c-Abl inhibitor that is currently under clinical trial [19] forms only three H-bonds with c-Abl (Figure not shown). DB04739, DB07326, and DB11841 are also predicted to penetrate the BBB. Lastly, the binding score of DB04739, DB07326, and DB11841 are − 11.8 kcal/mol, − 11.8 kcal/mol, and − 10.8 kcal/mol, respectively. When compared to nilotinib (− 14.2 kcal/mol), these molecules have low affinity to c-Abl. Based on these combined analyses of binding poses, predicted BBB permeability, and binding score (Kcal/mol) DB04868, DB04739, DB07326, and DB11841 were selected for molecular dynamics simulation (Table 1).

MM-GBSA analysis

The MM-GBSA was carried out for post-docking energy minimization to predict the free energy of binding (ΔG bind) for the set of ligands in complex with the receptor. From MM/GBSA results, the ΔG bind values were observed in the range of − 103.81 kcal/mol (DB04868) to − 70.12 kcal/mol (DB11841). The ΔCoul values were observed in the range of − 38.68 kcal/mol (DB04868) to − 12.01 kcal/mol (DB11841). The ΔH-bond values were

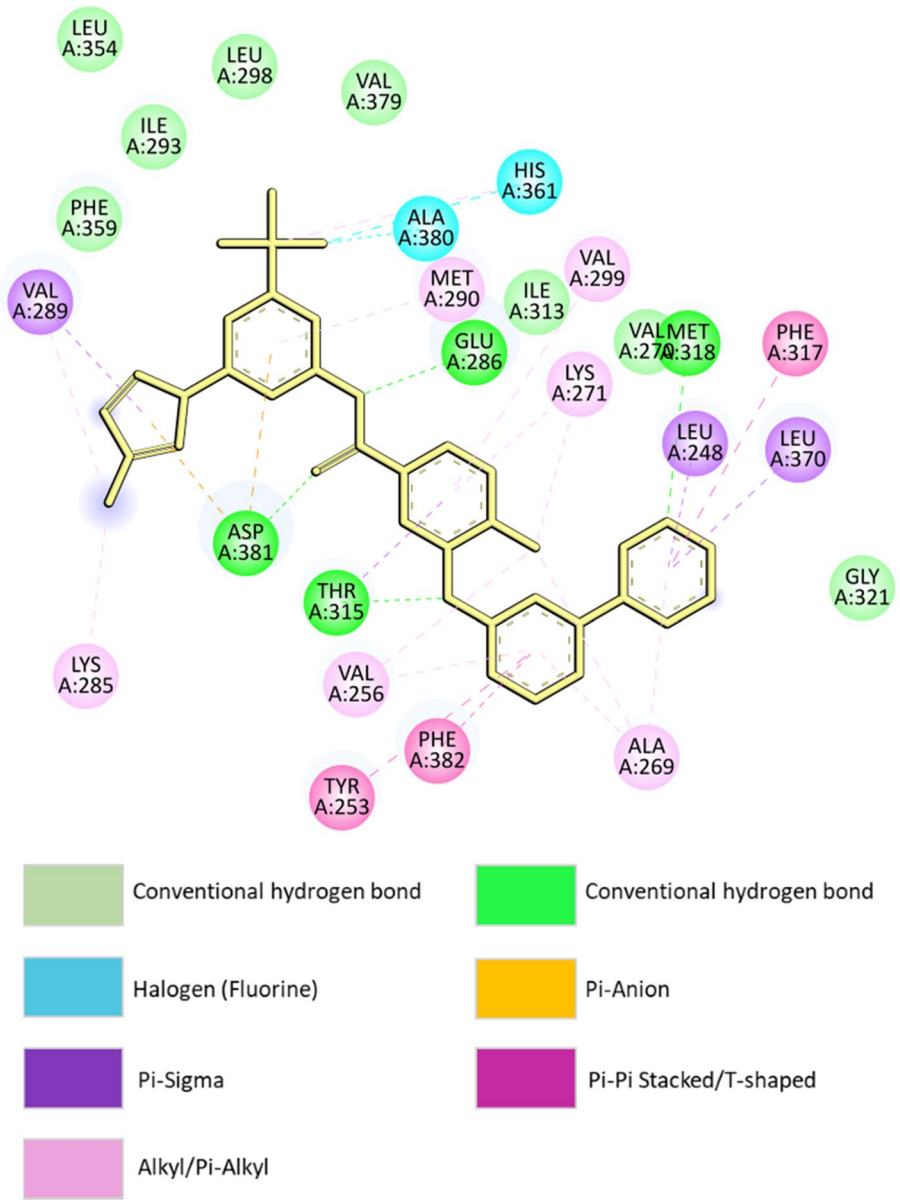

Fig. 1 Amino acids around nilotinib interact and form the binding pocket of c-Abl. The 2D interaction was visualized using discovery studio visualizer (v16.1.0.15350)

observed in the range of − 1.63 kcal/mol (DB04868) to − 3.62 kcal/mol (DB11841). The ΔLipo values were observed in the range of − 24.82 kcal/mol (DB07326) to − 33.16 kcal/mol (DB11841). Lastly, the ΔvdW values were observed in the range of − 67.85 kcal/mol (DB04868) to − 49.69 kcal/mol (DB11841), Table 2.

ADME and toxicity analysis

The ADME results of the top hits, DB04739, DB07326, and DB11841 including nilotinib (DB04868) obtained from QikProp are represented in Table 3. Lipinski's rule of five was applied to assess the drug-likeness of the top hits. The rule states that molecules with molecular weight < 500 g/mol, $QPlogP_{o/w} < 5$, HBD ≤ 5, and HBA ≤ 10 are considered to be drug-like molecules. According to Lipinski's rule, all the three hit molecules showed drug-likeness, except for the control drug DB04868 which have two violations in molecular weight and $QPlogP_{o/w}$ criteria. Following the acceptable range criteria provided by QikProp module, DB04868 and DB07326 show good gut–blood barrier permeability with QPPCaco value > 500. All the molecules are good blood–brain barrier permeable within the acceptable QPlogBB range of − 3.0 to 1.2 and display no central nervous system activity. DB04739 and DB11841 were predicted to be aqueous permeable within an acceptable QPlogS range of − 6.5 to 0.5. The total solvent accessible surface area (SASA) of the all the hits is in an acceptable range of 300–1000. All the hit molecules display high human oral absorption above 75%. The toxicity results are presented in

Table 1 Docking score of ligands

Sr. no	DrugBank ID	Common name/ PubChem ID	Binding score (Kcal/mol)	BBB permeability prediction	H-bond
1.	DB04868	Nilotinib	− 14.2	Yes	Glu286, Thr315, Met318, Asp381
2.	DB06925	15,991,573	− 13.4	Yes	Glu286, Met318, Asp381
3.	DB17141	Vodobatinib	− 12.8	Yes	Glu286, Met318, Asp381
4.	DB00619	Imatinib	− 12.4	Yes	Thr315, Met318, Asp381
5.	DB04739	Norimatinib	− 11.8	Yes	Glu286, Thr315, Met318, Asp381
6.	DB07326	23,658,582	− 11.8	Yes	Glu286, Thr315, Met318, Asp381
7.	DB08091	5,326,868	− 11.8	Yes	Glu286, Met318, Met381
8.	DB16035	24,756,034	− 11.8	Yes	Glu286, Met318, Asp381
9.	DB08242	23,400,214	− 11.7	Yes	Glu286, Thr315, Asp381
10.	DB07537	24,812,718	− 11	Yes	Glu286, Met318, Asp381,
11.	DB07831	10,477,723	− 10.9	Yes	Glu286, Glu316, Met318
12.	DB12270	Losmapimod	− 10.7	Yes	Glu286, Met381
13.	DB11841	Entinostat	− 10.6	Yes	Glu286, Thr315, Met318, Asp381
14.	DB11903	10,253,143	− 10.6	Yes	Asp381
15.	DB06518	11,406,590	− 10.5	Yes	Glu286, Asp381
16.	DB11450	Pimobendan	− 10.4	Yes	Glu286, Glu316, Asp381
17.	DB07362	15,602,701	− 10.1	Yes	Glu286, Met318, Asp381
18.	DB07360	24,880,024	− 10.1	Yes	Glu286, Met318, Asp381
19.	DB06134	24,995,524	− 9.5	Yes	Glu286, Met318, Asp381
20.	DB12779	Higenamine	− 9.3	Yes	Glu286, Met318
21.	DB02647	449,088	− 8.9	Yes	Thr315, Glu316, Met318

Table 4. Various toxicity parameters were assessed such as hepatoxicity, carcinogenicity, immunotoxicity, mutagenicity, and cytotoxicity. The ProTox-II webtool uses algorithm of rat in vivo toxicity parameter training sets and provides probability score of a toxicity target with a remark of either 'inactive' or 'active.' Among the top hit molecules, DB11841 out-performs in all the toxicity prediction as 'inactive' with probability score more than 50%. The LD_{50} of DB04868, DB04739, DB1184, and DB07326 are 800 mg/kg, 100 mg/kg, 22 mg/kg, and 500 mg/kg. Based on LD_{50}, DB11841 is highly toxic when compared to DB04868, DB04739, and DB07326. This indicates that caution has to be taken while selecting the dose for DB11841 at preclinical and clinical levels.

Molecular dynamics

The sequence length of c-Abl is composed of 1130 amino acids (Uniprot Id: P00519). The amino acid sequence length of c-Abl (PDB ID: 3CS9) is from residues Asp233-Ser500. The secondary structure of c-Abl (3CS9) is composed of 27 random coils marked in gray, 18 turns in green, 17 alpha-helices in red, and 10 beta-sheets in blue (Fig. S2). The stability of the ligand–receptor complex was investigated by MD simulation using Desmond (Academic version). The MD simulation was carried out for 100 ns. The 100 ns simulation time was decided based on the stability of the apoprotein. Prior to simulation of protein–ligand complexes, a 100 ns simulation was fixed for the apoprotein. The 100 ns results show that the system is stable as indicated by RMSD and RMSF of the apoprotein (Fig. S3). For 3CS9-DB04886 complex (Fig. 3A), the RMSD of the protein is stable during the course of 100 ns simulation with minimal deviation from 70 to 80 ns. While the RMSD of DB04868 is stable from 0 to 60 ns but shows major deviation from 80 to 100 ns. Despite this major deviation of DB04868, the RMSD of DB04868 at the end of simulation, 1.3 Å, is lower than that of the RMSD of protein, 2.2 Å. For 3CS9-DB04739 complex (Fig. 3B), the RMSD of protein shows deviation from 0 to 20 ns. Thereafter, the RMSD of protein is stable till the end of 100 ns simulation, while the RMSD of ligand shows major deviation from 0 ns to 40 and, thereafter, shows no major deviation till the end of simulation. However, the RMSD of ligand is larger, 3.5 Å, than that of protein 2.8 Å. This indicates that the ligand might have deviated from the ligand-binding site of the protein. For 3CS9-DB11841 complex (Fig. 3C), the RMSD of protein is similar to that of 3CS9-DB04868 complex and show no major deviation during the course of 100 ns simulation. While the ligand shows major deviation from 25 to 40 ns and, thereafter, stable till the end of simulation with the RMSD converging at 1.5 Å. Lastly, for 3CS9-DB07326 complex (Fig. 3D), the RMSD of

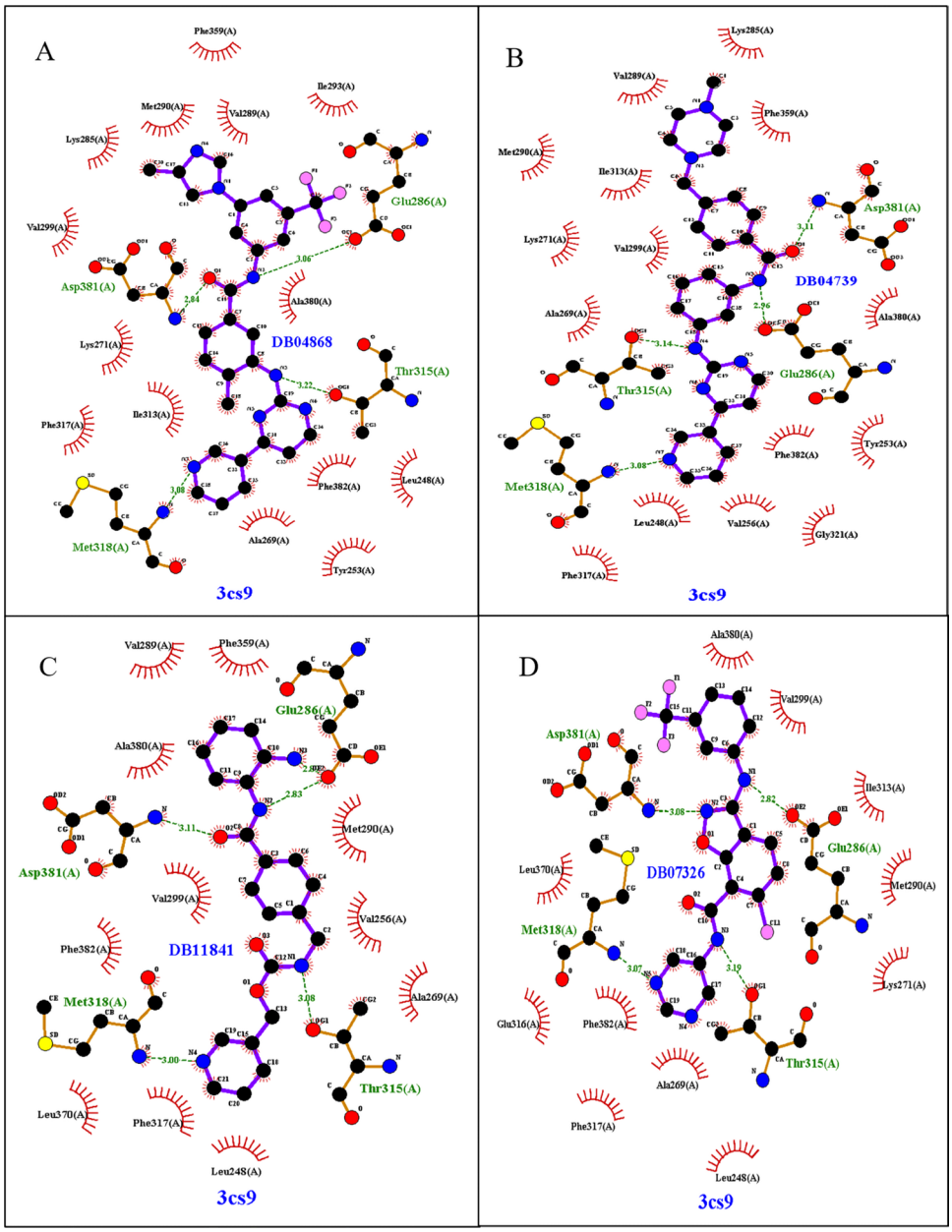

Fig. 2 The 2D diagrammatical representation of ligand–receptor interaction. **A** DB04868-3CS9 2D interactions. **B** DB04739-3CS9 2D interactions. **C** DB11841-3CS9 2D interactions. **D** DB07326-3CS9 2D interactions. All the ligands including the co-crystal ligand form H-bond with Glu286, Thr315, Met318, and Asp381. All interactions were visualized in LigPlot+ v.2.2

Table 2 MM-GBSA results of top hits

Sr. no	Compound name/ID	Δ*G* bind (Kcal/mol)	ΔCoul (Kcal/mol)	Δ*H*-bond (Kcal/mol)	ΔLipo (Kcal/mol)	ΔvdW (Kcal/mol)
1.	DB04868	− 103.81	− 38.68	− 1.63	− 32.71	− 67.85
2.	DB04739	− 80.39	− 16.14	− 2.91	− 35.70	− 64.54
3.	DB11841	− 70.12	− 12.01	− 3.62	− 33.16	− 49.69
4.	DB07326	− 72.15	− 13.16	− 2.10	− 24.82	− 60.43

protein is similar to that of 3CS9-DB04868 complex (2.1 Å). For ligand, the RMSD deviated abruptly at around 37 ns and, thereafter, is stable till the end of the simulation with the RMSD of 0.8 Å.

RMSF determines the fluctuation (movement) of each amino acids during the simulation. The higher the fluctuation, the lower the stability of ligand–protein contact and vice versa. Figure 4 shows the fluctuations of amino acids,

Table 3 ADME prediction of top hits

Compound name	Mol.Wt[a]	HBD[b]	HBA[c]	QPPCaco[d]	QPlogBB[e]	QPPMDCK[f]	CNS[g]	QPlogS[h]	QPlog$P_{o/w}$[i]	SASA[j]	% Human oral absorption[k]
DB04868	529.523	2	8	777.648	−0.622	1663.567	−1	−6.969	5.14	769.116	82.864
DB04739	479.583	2	10.5	66.53	−0.188	32.354	1	−3.728	3.067	822.448	77.533
DB11841	376.414	3.5	7.5	208.337	−1.765	90.785	−2	−5.057	2.749	702.722	84.543
DB07326	433.776	2	7.5	548.509	−0.656	2457.567	0	−6.064	3.568	680.267	96.865

[a]Molecular weight (< 130.0–725.0 g/mol)

[b]Hydrogen bonds that would be donated by the solute to water molecules in an aqueous solution (0.0–6.0)

[c]Hydrogen bonds that would be accepted by the solute from water molecules in an aqueous solution

[d]Gut–blood barrier permeability prediction for non-active transport molecules (< 25 poor, > 500 great)

[e]Brain/blood partition coefficient prediction for orally delivered drugs (–3.0 to 1.2)

[f]Blood–brain barrier prediction for non-active transport (< 25 poor, > 500 great)

[g]Predicted central nervous system activity [−2 (inactive) to +2 (active)]

[h]Aqueous solubility prediction (−6.5 to 0.5)

[i]Octanol/water partition coefficient prediction (−2.0 to 6.5)

[j]Total solvent accessible surface area (SASA) (300–1000)

[k]Predicted human oral absorption on 0–100% scale (> 80% high and < 20% poor)

Table 4 Toxicity prediction report of DB04868, DB04739, DB11841, and DB07326

DrugBank ID	Toxicity target and their probability score					LD_{50} (mg/kg)
	Hepatotoxicity	Carcinogenicity	Immunotoxicity	Mutagenicity	Cytotoxicity	
DB04868	Active (0.82)	Active (0.53)	Active (0.98)	Inactive (0.59)	Inactive (0.72)	800 54.26
DB04739	Active (0.55)	Inactive (0.65)	Active (0.77)	Inactive (0.76)	Inactive (0.65)	100 54.26
DB11841	Inactive (0.72)	Inactive (0.53)	Inactive (0.97)	Inactive (0.67)	Inactive (0.84)	22 68.07
DB07326	Active (0.72)	Active (0.54)	Inactive (0.77)	Active (0.51)	Inactive (0.81)	500 54.26

Glu286, Thr315, Met318, and Asp381 that form H-bonds with all DB04868, DB04739, DB11841, and DB07326 falls within 1.2 Å. For 3CS9-DB04868 complex, the RMSF of amino acids, Glu286, Thr315, Met318, and Asp381 of protein that forms H-bonds with DB04868 falls within 1 Å. For 3CS9-DB04739, 3CS9-DB11841, and 3CS9-DB07326 complexes, the RMSF of amino acids Thr315, Met318, and Asp381 is within 1 Å, while Glu286, when compared to Thr315, Met318, and Asp381, shows a small fluctuation with RMSF of 1.2 Å. The fluctuation with Glu286 is higher when compared to Thr315, Met318, and Asp381 because the H-bond formed with Glu286 is weakly retain during the 100 ns simulation. Additionally, a critical observation was observed with different regions (R1, R2, R3) of the protein when the top hits bind to it. The regions R1, R2, and R3 were significantly stabilized by the binding of DB11841 when compared to the reference molecule (DB04868), while, the other two hits, DB04739 and DB07326, significantly stabilized only R3 when compared to the reference molecule (DB04868). The regions R1, R2, and R3 are composed of random coils and turns of secondary structure. These regions were designated as loops 1, 2, and 3 (Fig. S2). R1 is composed of seven amino acid residues of which five, i.e., Leu273, Lys274, Thr277, Met278, and Glu279 represent coils, and two amino acid residues i.e., Glu275 and Asp276 represent turns. Similarly, R2 is composed of seven amino acid residues of which one i.e., Leu387 represents turn, and six, i.e., Met388, Thr389, Gly390, Asp391, Thr392, Tyr393 represent coils. R3 is composed of 12 amino acid residues. Of these four amino acid residues, i.e., Lys454, Asp455, Glu462, Gly463 represent turns, and eight amino acid residues, i.e., Tyr456, Arg457, Met458, Glu459, Arg460, Pro461, Ala464, Cys465 represent coils. Secondary structure elements like alpha-helices and beta-sheets are usually more rigid and fluctuate the least when compared to the unstructured parts of the protein, i.e., loop regions, N- and C-terminal of the proteins.

The ligand interaction fractions of ligands with amino acids of c-Abl during a span of 100 ns are depicted in Fig. 5. As shown in Fig. 5, hydrophobic and H-bond are the dominant interactions. DB04868 retains more than 70% of H-bond interaction with Glu286, Thr315, Met318, and Asp381 during the 100 ns simulation. DB04739 retains more than 70% of H-bond interaction with Thr315, Met318,

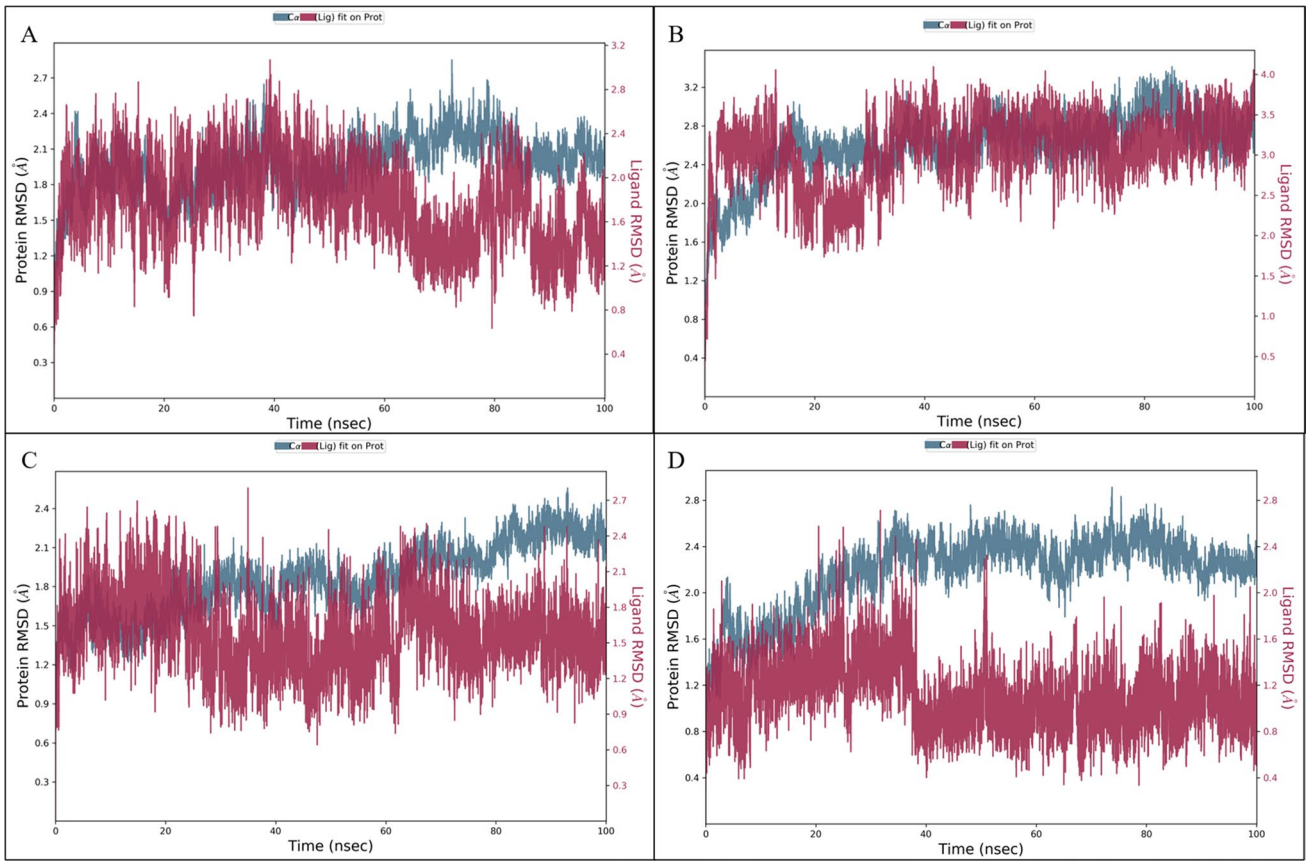

Fig. 3 The RMSD graph for the 100 ns simulation trajectory of ligand–receptor complex. **A** DB04868-3CS9 RMSD. **B** DB04739-3CS9 RMSD. **C** DB11841-3CS9 RMSD. **D** DB07326-3CS9 RMSD

and Asp381 but displays less than 10% of H-bond interaction with GLU286 during the 100 ns simulation. DB11841 retains more than 40% of H-bond interaction with GLU286, Thr315, and Met318 but displays less than 40% of H-bond interaction with Asp381 during the 100 ns simulation. Lastly, DB07326 retains more than 60% of H-bond interaction with Met318 and Asp381 but displays less than 20% of H-bond interaction Glu286 and Thr315. The ligand–protein 2D interactions following the 100 ns are depicted in Fig. 5. Overall, Fig. 6 shows that the critical amino acids of protein that majorly formed H-bond with nitrogen and amino groups of the ligands. In some cases, the H-bond is mediated by water molecules.

DFT analysis

The visualization of the optimized top hits DB04739, DB07326, and DB11841 including nilotinib (DB04868) was obtained using Chemcraft package (v1.8), and the result is presented in Fig. 7. The DFT calculations of the top hit molecules were optimized at B3LYP/6-31 G (d, p) basis set in the gas phase. The ($\Delta E_{\mathrm{HOMO}^{-}\mathrm{LUMO}}$) of the top hits is arranged in ascending order: DB04739 (3.8 eV) < DB07326 (4.11 eV) < DB04868 (4.13 eV) < DB11841 (4.42 eV) (Fig. 8). Among the top hits, DB04739 showed that least energy gap of 3.8 eV implies the high chemical reactivity.

Discussion

PD is the most common movement disorder [2]. PD is majorly linked with the depletion of dopamine form substantia nigra leading to disruption of substantia nigra-striatum pathway [1]. Pathologically, α-synuclein has been found in numerous brain specimens obtained from preclinical and clinical studies [16, 52]. α-synuclein contributes to PD by activation of non-neuronal cells [53], blocking the synaptic transport of dopamine [16], and increases the oxidation of dopamine [16]. Therefore, current studies have focused on targeting α-synuclein [54]. Similarly, studies of molecules that target upstream regulators of α-synuclein are being investigated.

c-Abl is a tyrosine kinase that is majorly expressed in cancer cells [26, 55]. Similarly, c-Abl expression has been shown to elevated in PD. Increased c-Abl expression activates α-synuclein and also increases the expression of

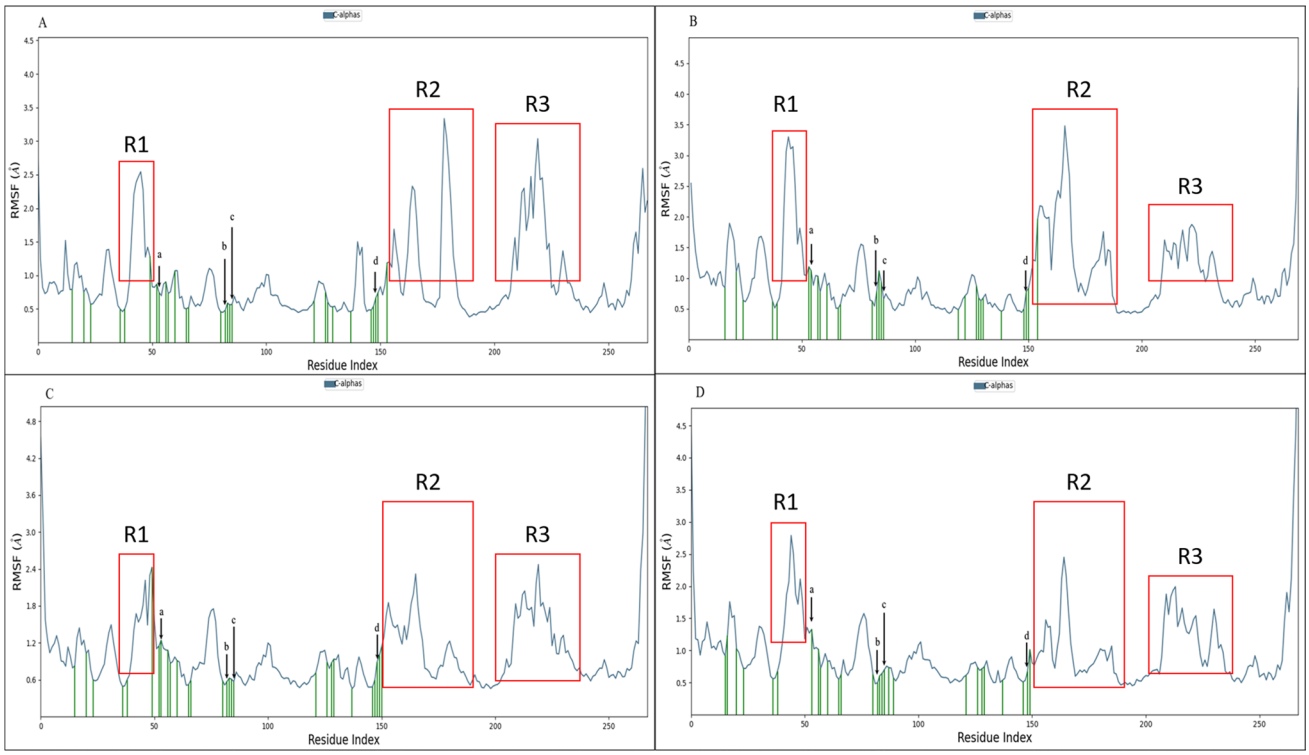

Fig. 4 The RMSF graph for the 100 ns simulation trajectory of ligand–receptor complex. **A** DB04868-3CS9 RMSD. **B** DB04739-3CS9 RMSD. **C** DB11841-3CS9 RMSD. **D** DB07326-3CS9 RMSD. [a]Glu286, [b]Thr315, [c]Met318, [d]Asp381

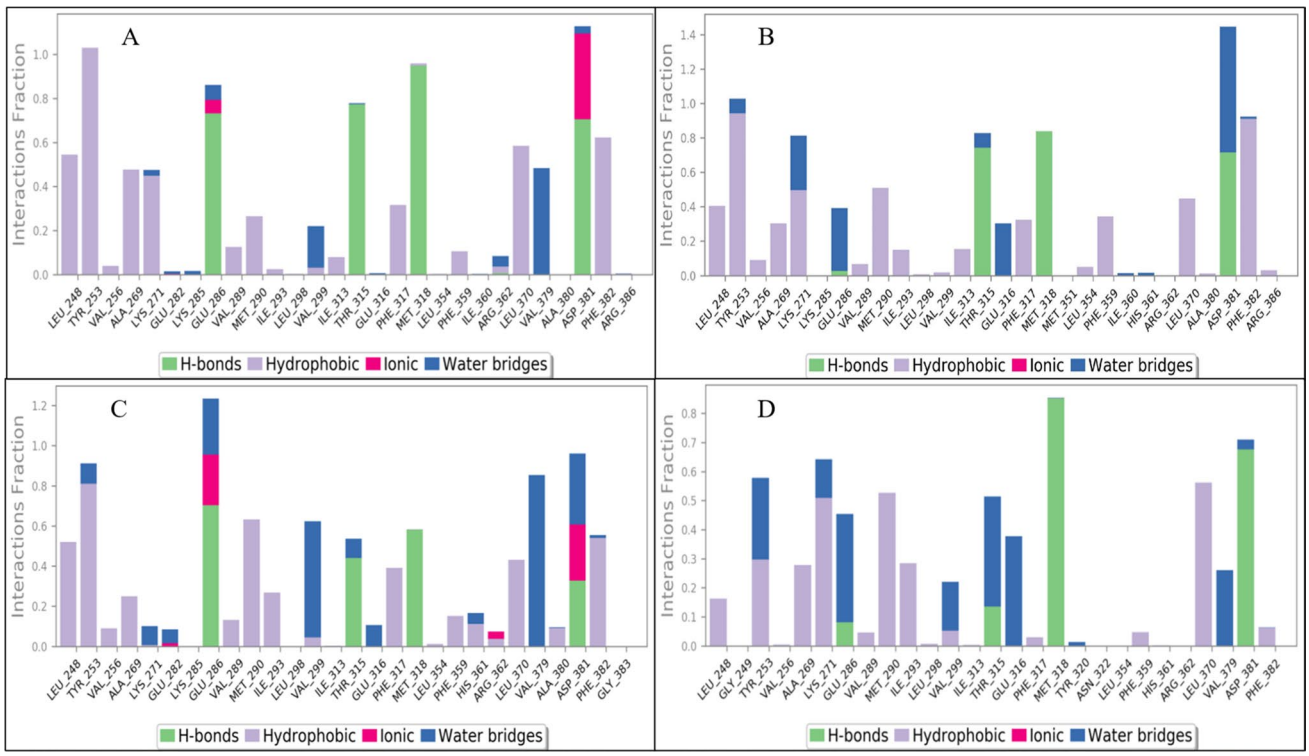

Fig. 5 The ligand interaction fractions graph of ligands with amino acids of 3CS9 for the 100 ns simulation trajectory. **A** DB04868-3CS9 ligand interaction fraction. **B** DB04739-3CS9 ligand interaction fraction. **C** DB11841-3CS9 ligand interaction fraction. **D** DB07326-3CS9 ligand interaction fraction

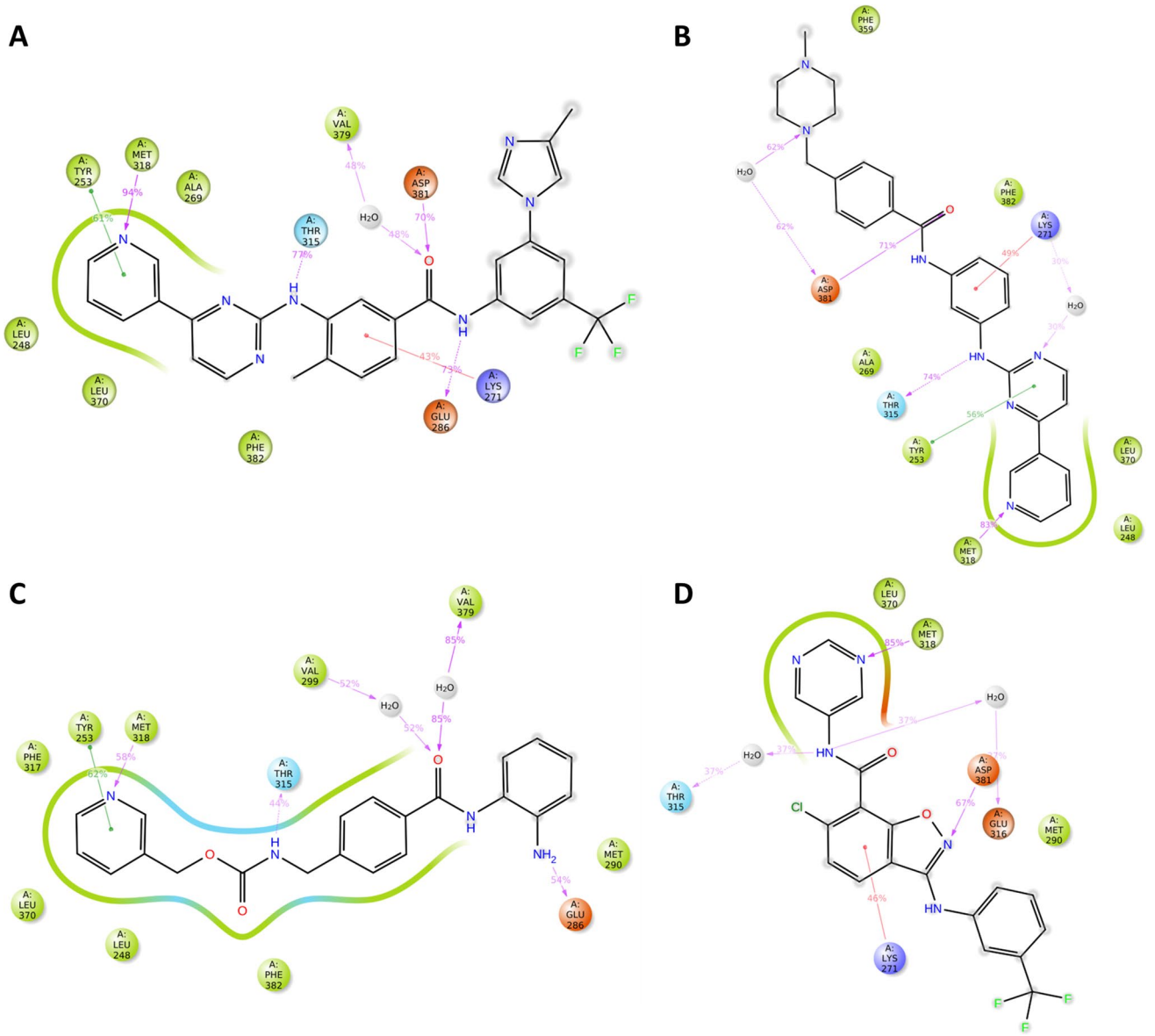

Fig. 6 The 2D interaction diagram of ligand–receptor complex for the 100 ns simulation trajectory. **A** DB04868-3CS9 2D interactions. **B** DB04739-3CS9 2D interactions. **C** DB11841-3CS9 2D interactions. **D** DB07326-3CS9 2D interactions

α-synuclein, thereby contributing to PD development [31, 33]. In line with the above observations, several studies have shown to decreased the activation and expression of α-synuclein upon inhibition of c-Abl [31, 33]. Currently, nilotinib [29, 36] and vodobatinib [27] are being investigated for PD.

In this study, three molecules, DB04739 (norimatinib), DB07326, and DB11841 (entinostat) were identified as potential c-Abl inhibitors through molecular docking and molecular dynamics studies. The overall results of these molecules were compared with nilotinib that is complexing with protein (PBD ID 3CS9). Based on molecular docking studies and BBB permeability prediction, 21 hits were short-listed analysis. Molecular docking studies show that nilotinib is having a better binding affinity of − 14.2 kcal/mol. This was followed by DB06925, vodobatinib, imatinib with binding affinity of − 13.4 kcal/mol, 12.8 kcal/mol, and 12.4 kcal/mol, respectively. While the binding affinity of norimatinib, DB07326, and entinostat were − 11.8 kcal/mol, − 11.8 kcal/mol, and − 10.8 kcal/mol, respectively. Insights into the 2D interactions of orimatinib, DB07326, and entinostat indicate that molecules form H-bond with the same residues (Glu286, Thr315, Met318, Asp381) that interacts with nilotinib [56]. MM-GBSA studies indicate that Δ*G* bind, ΔCoul, Δ*H*-bond, ΔLipo, and ΔvdW are positively contributing to the

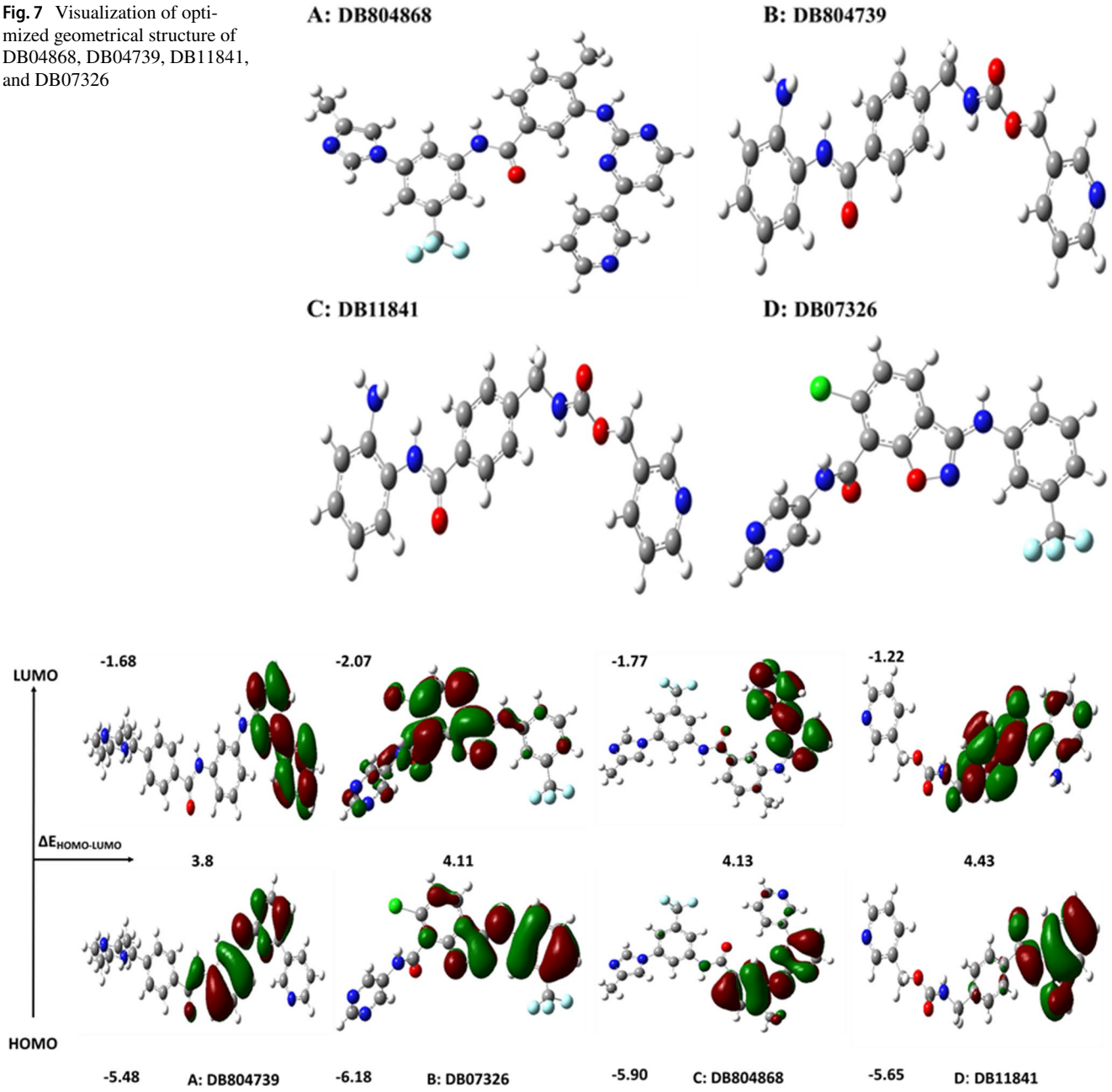

Fig. 7 Visualization of optimized geometrical structure of DB04868, DB04739, DB11841, and DB07326

Fig. 8 E_{HOMO} and E_{LUMO} mapping of DB04868, DB04739, DB11841, and DB07326. Blue color indicates positive potential. Red color—negative potential

ligand–receptor binding. ADME prediction by QikProp module, Schrodinger revealed that all the hit molecules follow Lipinski's rule of five and is estimated to have good human oral bioavailability above 75% when compared to the standard, DB04848. All the molecules display good blood–brain permeability within an acceptable QPlogBB range of − 3.0 to 1.2. The ADME parameters of the hits such as aqueous solubility prediction and total solvent accessible surface area display acceptable range. DFT calculation indicates that DB04739 is having the lowest energy gap when compared to other hits. This indicates that DB04739 is likely to be reactive when compared to other hits. However, toxicity prediction revealed that DB04868, DB04739, and DB07326 exhibit toxicity signs such as hepatoxicity, carcinogenicity, mutagenicity, immunotoxicity, and cytotoxicity. In contrast, DB11841 shows no signs of toxicity, suggesting its potential as a drug candidate for both preclinical and clinical assessments in PD. However, it is crucial to note that LD_{50} prediction urges careful dosage selection for this compound.

Based on the 2D interactions, BBB prediction and binding affinity DB04739, DB07326, and DB11841 were further selected for molecular dynamics studies. Molecular dynamics studies show that norimatinib, DB07326, and entinostat are all stable during the course of 100 ns simulation. RMSD of the protein and the ligands fall within the acceptable range (< 2.5 Å). Similarly, the RMSF of protein, particular in the positions which coincides with the key amino acids (Glu286, Thr315, Met318, Asp381) that forms H-bond is minimal (< 1.5 Å). A low RMSF value in the binding site of amino acids, especially those that participated in H-bond formation, indicates that these residues make strong interactions with the small molecule with minimal deviation from its initial location at an atomistic level in the simulation trajectory. This results in optimal binding between the small molecule and the protein. The ligand interaction fractions of the three ligands, norimatinib, DB07326, and entinostat, are comparable to that of nilotinib except the contact of norimatinib with Glu286 which is too weak (< 10%).

DB04868 (nilotinib) is a multi-kinase inhibitor that is preferentially targeting Abl. Nilotinib has been reported to inhibit misfolded proteins including α-synuclein in several neurodegenerative models. Nilotinib is clinical approved drug for the treatment of chronic myeloid leukemia [29]. DB04739 (norimatinib) is an active metabolite of imatinib that is being investigated as potential anticancer agent. Both imatinib and norimatinib have shown to inhibit Abl and thereby prevent cancer growth [57, 58]. However, unlike imatinib, norimatinib has been shown to have a weak anticancer activity [58]. DB07326 is an experimental molecule. It is a potent and selective c-Kit inhibitor that was discovered as a possible agent for the treatment of inflammatory and autoimmune diseases [59]. DB11841 (entinostat) belongs to a class of molecule that inhibits histone deacetylase. It is currently under clinical trials (NCT02115282, NCT05053971, NCT03250273) and is being investigated as a possible agent for the treatment of several cancer.

Conclusion

In summary, three molecules namely DB04739 (norimatinib), DB07326, and DB11841 (entinostat) were identified as potential inhibitor of c-Abl protein. These molecules interact with key amino acids of c-Abl that are shown to interact with Nilotinib. Based on molecular docking, DB04739, DB07326, and DB11841 were further selected for MD simulation. Among these three molecules, DB04739 and DB11841 interact the least with Glu286 (< 10%). Other than Glu286, Thr315, Met316, and Asp381, DB04739, DB07326, and DB11841 are able to form additional H-bond to other amino acids that are mediated by water. These observations highlight the additional benefits of DB04739, DB07326, and DB11841 over nilotinib and could be potential agents for targeting c-Abl in PD. Furthermore, based on DFT studies, DB04739 is likely to exhibit reactivity in comparison to other hits. In addition, toxicity prediction indicates that DB11841 shows no signs of toxicity, making it a potential candidate for preclinical and clinical testing in PD. In conclusion, our current study is limited to in silico findings. Further in vitro and in vivo studies on PD models focusing on toxicities, efficacy, and safety of the reported molecules are warranted. In addition, the neuroprotective or disease-modifying studies emphasizing on the ability of the reported molecules to inhibit c-Abl for the prevention of PD is required to confirm the findings highlighted herewith.

Supplementary Information The online version contains supplementary material available at https://doi.org/10.1007/s11030-023-10796-3.

Acknowledgements The author would like to thank the Department of Science and Technology—Fund for Improvement of Science and Technology Infrastructure in Universities and Higher Educational Institutions (DST-FIST), New Delhi for their infrastructure support to our department. The author would also like to express a special thanks to the management of JSS College of Pharmacy, Ooty and JSS Academy of Higher Education & Research, Mysuru.

Author contributions ER performed the literature review, designed the concept, performed the study, and interpretation of results. DR performed the study, interpretation of results, and edited the manuscript. SJ and VS performed and interpreted the DFT studies. All the authors approved the final manuscript for submission and publication.

Funding The study did not receive any funding for carrying out the work.

Declarations

Conflict of interest The author declares no conflict of interest.

References

1. Poewe W, Seppi K, Tanner CM et al (2017) Parkinson disease. Nat Rev Dis Prim 3:1–21. https://doi.org/10.1038/nrdp.2017.13
2. Pang SYY, Ho PWL, Liu HF et al (2019) The interplay of aging, genetics and environmental factors in the pathogenesis of Parkinson's disease. Transl Neurodegener 8:1–11
3. Dye RV, Miller KJ, Singer EJ, Levine AJ (2012) Hormone replacement therapy and risk for neurodegenerative diseases. Int J Alzheimers Dis. https://doi.org/10.1155/2012/258454
4. Pinto JM, Castillo RL, Sotomayor-Zárate R (2018) Sex hormones: role in neurodegenerative diseases and addiction. In: Sex hormones in neurodegenerative processes and diseases. 207–224. https://doi.org/10.5772/intechopen.71380
5. Villa A, Vegeto E, Poletti A, Maggi A (2016) Estrogens, neuroinflammation, and neurodegeneration. Endocr Rev 37:372–402
6. Lee YH, Cha J, Chung SJ et al (2019) Beneficial effect of estrogen on nigrostriatal dopaminergic neurons in drug-naïve postmenopausal Parkinson's disease. Sci Rep 9:10531–10539. https://doi.org/10.1038/s41598-019-47026-6

7. Masato A, Plotegher N, Boassa D, Bubacco L (2019) Impaired dopamine metabolism in Parkinson's disease pathogenesis. Mol Neurodegener 14:35
8. Zarow C, Lyness SA, Mortimer JA, Chui HC (2003) Neuronal loss is greater in the locus coeruleus than nucleus basalis and substantia nigra in Alzheimer and Parkinson diseases. Arch Neurol 60:337–341. https://doi.org/10.1001/archneur.60.3.337
9. Morale MC, Serra PA, L'Episcopo F et al (2006) Estrogen, neuroinflammation and neuroprotection in Parkinson's disease: glia dictates resistance versus vulnerability to neurodegeneration. Neuroscience 138:869–878. https://doi.org/10.1016/j.neuroscience.2005.07.060
10. Del Rey NLG, Quiroga-Varela A, Garbayo E et al (2018) Advances in Parkinson's disease: 200 years later. Front Neuroanat 12:1–14. https://doi.org/10.3389/fnana.2018.00113
11. Kalia LV, Lang AE (2015) Parkinson's disease. The Lancet 386:896–912
12. Dong XX, Wang Y, Qin ZH (2009) Molecular mechanisms of excitotoxicity and their relevance to pathogenesis of neurodegenerative diseases. Acta Pharmacol Sin 30:379–387
13. Iovino L, Tremblay ME, Civiero L (2020) Glutamate-induced excitotoxicity in Parkinson's disease: the role of glial cells. J Pharmacol Sci 144:151–164
14. Venda LL, Cragg SJ, Buchman VL, Wade-Martins R (2010) α-Synuclein and dopamine at the crossroads of Parkinson's disease. Trends Neurosci 33:559–568
15. Lohr KM, Masoud ST, Salahpour A, Miller GW (2017) Membrane transporters as mediators of synaptic dopamine dynamics: implications for disease. Eur J Neurosci 45:20–33. https://doi.org/10.1111/ejn.13357
16. Somayaji M, Lanseur Z, Choi SJ et al (2021) Roles for α-synuclein in gene expression. Genes (Basel) 12:1166. https://doi.org/10.3390/genes12081166
17. Fujioka S, Ogaki K, Tacik PM et al (2014) Update on novel familial forms of Parkinson's disease and multiple system atrophy. Parkinsonism Relat Disord. https://doi.org/10.1016/S1353-8020(13)70010-5
18. Rutherford NJ, Giasson BI (2015) The A53E α-synuclein pathological mutation demonstrates reduced aggregation propensity in vitro and in cell culture. Neurosci Lett 597:43–48. https://doi.org/10.1016/j.neulet.2015.04.022
19. Meade RM, Fairlie DP, Mason JM (2019) Alpha-synuclein structure and Parkinson's disease—lessons and emerging principles. Mol Neurodegener 14:29
20. Brahmachari S, Ge P, Lee SH et al (2016) Activation of tyrosine kinase c-Abl contributes to α-synuclein-induced neurodegeneration. J Clin Investig 126:2970–2988. https://doi.org/10.1172/JCI85456
21. Anderson JP, Walker DE, Goldstein JM et al (2006) Phosphorylation of Ser-129 is the dominant pathological modification of α-synuclein in familial and sporadic Lewy body disease. J Biol Chem 281:29739–29752. https://doi.org/10.1074/jbc.M600933200
22. Na CH, Sathe G, Rosenthal LS et al (2020) Development of a novel method for the quantification of tyrosine 39 phosphorylated α- and β-synuclein in human cerebrospinal fluid. Clin Proteomics 17:1–9. https://doi.org/10.1186/s12014-020-09277-8
23. Madsen DA, Schmidt SI, Blaabjerg M, Meyer M (2021) Interaction between parkin and α-synuclein in park2-mediated Parkinson's disease. Cells 10:1–30
24. Chung E, Choi Y, Park J et al (2020) Intracellular delivery of Parkin rescues neurons from accumulation of damaged mitochondria and pathological α-synuclein. Sci Adv 6:1–15. https://doi.org/10.1126/sciadv.aba1193
25. Yasuda T, Hayakawa H, Nihira T et al (2011) Parkin-mediated protection of dopaminergic neurons in a chronic MPTP-minipump mouse model of Parkinson disease. J Neuropathol Exp Neurol 70:686–697. https://doi.org/10.1097/NEN.0b013e3182269ecd
26. Hantschel O, Superti-Furga G (2004) Regulation of the c-Abl and Bcr-Abl tyrosine kinases. Nat Rev Mol Cell Biol 5:33–44
27. Walsh RR, Damle NK, Mandhane S et al (2023) Plasma and cerebrospinal fluid pharmacokinetics of vodobatinib, a neuroprotective c-Abl tyrosine kinase inhibitor for the treatment of Parkinson's disease. Parkinsonism Relat Disord 108:105281. https://doi.org/10.1016/j.parkreldis.2023.105281
28. Turner RS, Hebron M, Lawler A et al (2020) Nilotinib effects on safety, tolerability, and biomarkers in Alzheimer's disease: a phase 2, double-blind, randomized, placebo-controlled trial. Alzheimers Dement 16:309–317. https://doi.org/10.1002/alz.044628
29. Pagan FL, Hebron ML, Wilmarth B et al (2020) Nilotinib effects on safety, tolerability, and potential biomarkers in Parkinson disease: a phase 2 randomized clinical trial. JAMA Neurol 77:309–317. https://doi.org/10.1001/jamaneurol.2019.4200
30. Turner RS, Hebron ML, Lawler A et al (2020) Nilotinib effects on safety, tolerability, and biomarkers in Alzheimer's disease. Ann Neurol 88:183–194. https://doi.org/10.1002/ana.25775
31. Mahul-Mellier AL, Fauvet B, Gysbers A et al (2014) C-Abl phosphorylates α-synuclein and regulates its degradation: implication for α-synuclein clearance and contribution to the pathogenesis of Parkinson's disease. Hum Mol Genet 23:2858–2879. https://doi.org/10.1093/hmg/ddt674
32. Werner MH, Olanow CW (2022) Parkinson's disease modification through Abl kinase inhibition: an opportunity. Mov Disord 37:6–15
33. Brahmachari S, Karuppagounder SS, Ge P et al (2017) C-Abl and Parkinson's disease: mechanisms and therapeutic potential. J Parkinsons Dis 7:589–601
34. Imam SZ, Trickler W, Kimura S et al (2013) Neuroprotective efficacy of a new brain-penetrating C-Abl inhibitor in a murine Parkinson's disease model. PLoS ONE 8:e65129. https://doi.org/10.1371/journal.pone.0065129
35. Hebron ML, Lonskaya I, Moussa CEH (2013) Nilotinib reverses loss of dopamine neurons and improves motor behavior via autophagic degradation of α-synuclein in Parkinson's disease models. Hum Mol Genet 22:3315–3328. https://doi.org/10.1093/hmg/ddt192
36. Pagan FL, Hebron ML, Wilmarth B et al (2019) Pharmacokinetics and pharmacodynamics of a single dose Nilotinib in individuals with Parkinson's disease. Pharmacol Res Perspect 7:1–12. https://doi.org/10.1002/prp2.470
37. Lopez-Cuina M, Guerin PA, Canron MH et al (2020) Nilotinib fails to prevent synucleinopathy and cell loss in a mouse model of multiple system atrophy. Mov Disord 35:1163–1172. https://doi.org/10.1002/mds.28034
38. Ahamad S, Hema K, Gupta D (2023) Identification of novel tau-tubulin kinase 2 inhibitors using computational approaches. ACS Omega 8:13026–13037. https://doi.org/10.1021/acsomega.3c00225
39. Ahamad S, Kanipakam H, Kumar V, Gupta D (2021) A molecular journey to check the conformational dynamics of tau tubulin kinase 2 mutations associated with Alzheimer's disease. RSC Adv 11:1320–1331. https://doi.org/10.1039/d0ra07659g
40. Ahamad S, Hema K, Kumar V, Gupta D (2021) The structural, functional, and dynamic effect of tau tubulin kinase1 upon a mutation: a neuro-degenerative hotspot. J Cell Biochem 122:1653–1664. https://doi.org/10.1002/jcb.30112
41. Oleg T, Arthur JO (2010) AutoDock Vina: improving the speed and accuracy of docking with a new scoring function, efficient optimization, and multithreading. J Comput Chem 31:455–461
42. Selvaraj D, Muthu S, Kotha S et al (2021) Syringaresinol as a novel androgen receptor antagonist against wild and mutant androgen receptors for the treatment of castration-resistant prostate

cancer: molecular docking, in-vitro and molecular dynamics study. J Biomol Struct Dyn 39:621–634. https://doi.org/10.1080/07391102.2020.1715261
43. Liu H, Wang L, Lv M et al (2014) AlzPlatform: an Alzheimer's disease domain-specific chemogenomics knowledgebase for polypharmacology and target identification research. J Chem Inf Model 54:1050–1060. https://doi.org/10.1021/ci500004h
44. Chinnasamy S, Nagamani S, Muthusamy K (2015) Zn^{2+} ion of the snake venom metalloproteinase (SVMP) plays a critical role in ligand binding: a molecular dynamics simulation study. RSC Adv 5:70566–70576. https://doi.org/10.1039/c5ra14693c
45. Nagamani S, Muthusamy K, Marshal JJ (2016) E-pharmacophore filtering and molecular dynamics simulation studies in the discovery of potent drug-like molecules for chronic kidney disease. J Biomol Struct Dyn 34:2233–2250. https://doi.org/10.1080/07391102.2015.1111168
46. Banerjee P, Eckert AO, Schrey AK, Preissner R (2018) ProTox-II: a webserver for the prediction of toxicity of chemicals. Nucleic Acids Res 46:W257–W263. https://doi.org/10.1093/nar/gky318
47. Al Otaibi AA, Alshammari SL, Dhahi Alsukaibi AK et al (2023) Synthesis, anticancer activity, molecular docking and molecular dynamics studies of some pyrazole–chalcone hybrids. J Biomol Struct Dyn. https://doi.org/10.1080/07391102.2023.2199867
48. Alshammari MM, Soury R, Alenezi KM et al (2022) Synthesis, characterization, anticancer and in silico studies of a pyrazole-tethered thiazolidine-2,4-dione derivative. J Biomol Struct Dyn 40:13075–13082. https://doi.org/10.1080/07391102.2021.1981451
49. Agwupuye JA, Louis H, Gber TE et al (2022) Molecular modeling and DFT studies of diazenylphenyl derivatives as a potential HBV and HCV antiviral agents. Chem Phys Impact 5:1–13. https://doi.org/10.1016/j.chphi.2022.100122
50. Kirubakaran P, Karthikeyan M (2013) Pharmacophore modeling, 3D-QSAR and DFT studies of IWR small-molecule inhibitors of Wnt response. J Recept Signal Transduct 33:276–285. https://doi.org/10.3109/10799893.2013.822888
51. (1979) Frontier orbitals and organic chemical reactions. J Mol Struct 56:306. https://doi.org/10.1016/0022-2860(79)80172-6
52. Zhang J, Li X, Da LJ (2019) The roles of post-translational modifications on α-synuclein in the pathogenesis of Parkinson's diseases. Front Neurosci 13:381
53. Duffy MF, Collier TJ, Patterson JR et al (2018) Lewy body-like alpha-synuclein inclusions trigger reactive microgliosis prior to nigral degeneration. J Neuroinflamm. https://doi.org/10.1186/s12974-018-1171-z
54. Zella SMA, Metzdorf J, Ciftci E et al (2019) Emerging immunotherapies for Parkinson disease. Neurol Ther 8:29–44
55. Plattner R, Kadlec L, Demali KA et al (1999) c-Abl is activated by growth factors and Src family kinases and has a role in the cellular response to PDGF. Genes Dev 13:2400–2411. https://doi.org/10.1101/gad.13.18.2400
56. Weisberg E, Manley PW, Breitenstein W et al (2005) Characterization of AMN107, a selective inhibitor of native and mutant Bcr-Abl. Cancer Cell 7:129–141. https://doi.org/10.1016/j.ccr.2005.01.007
57. Iacuzzi V, Posocco B, Zanchetta M et al (2019) Development and validation of LC-MS/MS method for imatinib and norimatinib monitoring by finger-prick DBS in gastrointestinal stromal tumor patients. PLoS ONE 14:1–18. https://doi.org/10.1371/journal.pone.0225225
58. Mlejnek P, Dolezel P, Faber E, Kosztyu P (2011) Interactions of N-desmethyl imatinib, an active metabolite of imatinib, with P-glycoprotein in human leukemia cells. Ann Hematol 90:837–842. https://doi.org/10.1007/s00277-010-1142-7
59. Kunz RK, Rumfelt S, Chen N et al (2008) Discovery of amidobenzisoxazoles as potent c-Kit inhibitors. Bioorg Med Chem Lett 18:5115–5117. https://doi.org/10.1016/j.bmcl.2008.07.111